Quantitative CT Imaging of Carotid Arteries

11

Max J. van Gils, K. Hameeteman, M. van Straten, W.J. Niessen, and Aad van der Lugt

1 Background

Stroke is the second leading cause of mortality in the Western world after coronary heart disease. Although stroke death rate declined to 44 % in the last decade, the burden of disease remains high [1]. Of all strokes, 87 % are ischemic, 10 % are intracerebral hemorrhage and 3 % are subarachnoid hemorrhage strokes [1]. About 50 % of the ischemic strokes are due to atherosclerotic disease, which is preferentially located in the carotid artery [2].

Till now, the degree of luminal narrowing of the carotid arteries, caused by atherosclerosis, has been the only image-based risk factor for (recurrent) stroke that is used in therapeutic decision making. Large, randomized clinical trials (the North American Symptomatic Carotid Endarterectomy Trial (NASCET) and the European Carotid Surgery Trial (ECST)) have established the imaging criteria for surgical treatment in symptomatic patients. Carotid endarterectomy (CEA) is indicated for symptomatic patients with high-grade stenosis (>70 %) and in selected patients with recent symptoms and moderate stenosis (50–69 %) [3–5]. In asymptomatic carotid artery stenosis, a modest benefit of CEA is described in selected patient groups (relatively young male patients) who had a severe stenosis [6–8]. However, most patients with a stenosis >70 % are asymptomatic and most symptomatic patients have a carotid stenosis <70 %, which suggest that other factors play an important role in the pathophysiological cascade of ischemic stroke. Especially in the group of patients with moderate carotid stenosis, it is of clinical importance to improve risk prediction.

The last decades, extensive research has been performed to increase our knowledge of the pathophysiology of atherosclerosis. Apart from luminal narrowing of the carotid artery resulting in blood flow compromise, rupture of the atherosclerotic plaque and subsequent thromboembolism is thought to result in ischemic events. Histological studies of coronary arteries and carotid arteries have found that certain atherosclerotic plaque characteristics increase the vulnerability of the plaque to rupture. Inflammation is the hallmark of vulnerability and plaques with active inflammation may be identified by extensive macrophage infiltration. Plaques with a thin cap of <100 μm and a lipid core accounting for >40 % of total plaque volume are also considered highly vulnerable. Plaques with a fissured or ruptured cap are prone to thrombosis and thromboembolization [9]. Carotid plaque ulcerations on digital subtraction angiography (DSA) have been associated with plaque rupture [10] and with an increased risk of acute recurrent ischemic events [11, 12]. Advanced invasive and noninvasive imaging technologies enable the visualization of these atherosclerotic plaque characteristics in vivo.

DSA has long been the modality of choice for imaging carotid arteries, since it accurately visualizes the vascular lumen and its contours. However, DSA has several

Max J. van Gils (✉) • M. van Straten • Aad van der Lugt
Department of Radiology, Erasmus MC, University Medical Center Rotterdam, 'sGravendijkwal 230, 3015 CE Rotterdam, The Netherlands
e-mail: m.j.vangils@erasmusmc.nl; a.vanderlugt@erasmusmc.nl; marcel.vanstraten@erasmusmc.nl

K. Hameeteman
Biomedical Imaging Group Rotterdam, Department of Radiology, Erasmus MC, University Medical Center Rotterdam, Rotterdam, The Netherlands

Biomedical Imaging Group Rotterdam, Department of Medical Informatics, Erasmus MC, University Medical Center Rotterdam, Rotterdam, The Netherlands
e-mail: k.hameeteman@erasmusmc.nl

W.J. Niessen
Biomedical Imaging Group Rotterdam, Department of Radiology, Erasmus MC, University Medical Center Rotterdam, Rotterdam, The Netherlands

Biomedical Imaging Group Rotterdam, Department of Medical Informatics, Erasmus MC, University Medical Center Rotterdam, Rotterdam, The Netherlands

Imaging Science and Technology, Delft University of Technology, Delft, The Netherlands
e-mail: w.niessen@erasmusmc.nl

L. Saba et al. (eds.), *Multi-Modality Atherosclerosis Imaging and Diagnosis*,
DOI 10.1007/978-1-4614-7425-8_11,

disadvantages: it is invasive, laborious, time intensive, and expensive. Moreover, DSA requires skilled operators and is therefore less readily available. More importantly, cerebrovascular DSA has a non-negligible morbidity and mortality, with a complication rate of 0.4–12.2 % for neurological deficits [13, 14]. These drawbacks and the increasing interest in the arterial vessel wall have driven the use of other, less invasive modalities for imaging the carotid arteries.

Nowadays, noninvasive imaging techniques like duplex ultrasound (DUS), magnetic resonance imaging (MRI), and computed tomography (CT) not only enable grading of carotid stenosis but also provide a window to the atherosclerotic process in vivo [15]. They also allow for the quantification of plaque measures like plaque burden and plaque composition.

Using serial imaging, the early natural development of the atherosclerotic plaque can now be studied in vivo. Furthermore, it provides a tool to monitor changes in atherosclerotic plaque in response to secondary preventive therapies. The development of new pharmaceutical therapies is a slow and costly process, since the most reliable way to measure their clinical impact is to study its effect on clinical endpoints. The use of imaging biomarkers of atherosclerotic disease could speed up this process and reduce the number of subjects studied. For an effective use, imaging biomarkers should be derived in a robust, noninvasive way and the imaging modality should be broadly available [16]. Further, standardized image acquisition parameters and post-processing methods are required and the imaging biomarkers should be carefully validated and highly reproducible. The changes in an imaging biomarker should be correlated to the biological effect and the clinical endpoints [16]. Quantification, and especially automated quantification, of the degree of stenosis and atherosclerotic plaque measures is therefore important in the development of reliable surrogate endpoints for atherosclerosis.

Computed tomography angiography (CTA) is a potential imaging modality for monitoring atherosclerosis in vivo. It is a readily available and fast imaging technique causing minimal inconvenience for the patient. Although CTA involves potentially harmful ionizing radiation, the effective dose during a diagnostic CTA is relatively low (1–5 mSv) [17]. The increased acquisition speed of multidetector CT angiography (MDCTA) reduces motion artifacts. Current multidetector row CTA enables fast vascular imaging from the aortic arch to the intracranial vessels. This enables simultaneous investigation of other vascular territories, which makes that MDCTA can compete with other noninvasive imaging techniques and is increasingly used in the clinical evaluation of stroke patients. In this chapter, the state-of-the-art CTA technique used to evaluate carotid artery stenosis and atherosclerotic plaque is described.

2 Luminal Imaging Using CTA

2.1 Technical Aspects

In the early 1990s spiral CT was introduced, which enabled a volumetric data acquisition through continuous X-ray source rotation and simultaneous continuous table movement. Using this technique noninvasive imaging of blood vessels became widely available. The steady increase of the longitudinal coverage of the X-ray detectors, i.e., the number of slices, even further improved the feasibility of luminography.

Contrast material is necessary for the visualization of the lumen. Stenosis measurement relies upon the contrast difference between the lumen and its environment. Several technical factors should be taken into account when imaging vessel lumen using MDCTA.

The contrast difference between lumen and surrounding tissue is varying and depends mainly on the amount of lumen attenuation which is artificially increased by contrast material. The attenuation caused by contrast material can vary depending on patient-related factors like cardiac output and weight and on scan parameters and contrast protocol-specific factors. Peak tube voltage (kVp) influences the difference in HU values between different tissues. The lumen contrast density increases as tube voltage decreases. The lumen enhancement pattern is determined by the injection volume, the injection rate, and the iodine concentration in the contrast material [18]. Timing of contrast bolus arrival should be such that a maximum contrast density is achieved in the carotid artery with a concomitant low contrast density in the neighboring jugular vein. Use of a saline bolus chaser reduces the amount of contrast material needed by 20–40 % and reduces the extent of perivenous artifacts caused by a high contrast density in the jugular vein [18]. Synchronization between passage of the contrast bolus and data acquisition can be achieved by real-time bolus tracking at the level of the ascending aorta. Moreover, a craniocaudal scan direction also reduces contrast material-related perivenous artifacts [19]. The contrast injection protocol for carotid artery imaging is generally standardized with a fixed contrast volume of 80–125 mL (iodine concentration of >300 mg/mL) and a saline bolus chaser of 40 mL, both at an injection rate of 2–4 mL/s. The disadvantage of intravenous contrast in CT angiography remains its limited application in patients with renal insufficiency and hyperthyroidism.

Because of the limited spatial resolution of the CT scanner partial volume averaging occurs, leading to the so-called blooming artifact. This is easily appreciated at the boundary of the enhanced lumen and the vessel wall where differences in density are large. In subtle cases this is reflected in a blurred interface between structures as well. Partial volume averaging may influence the appreciation of the real lumi-

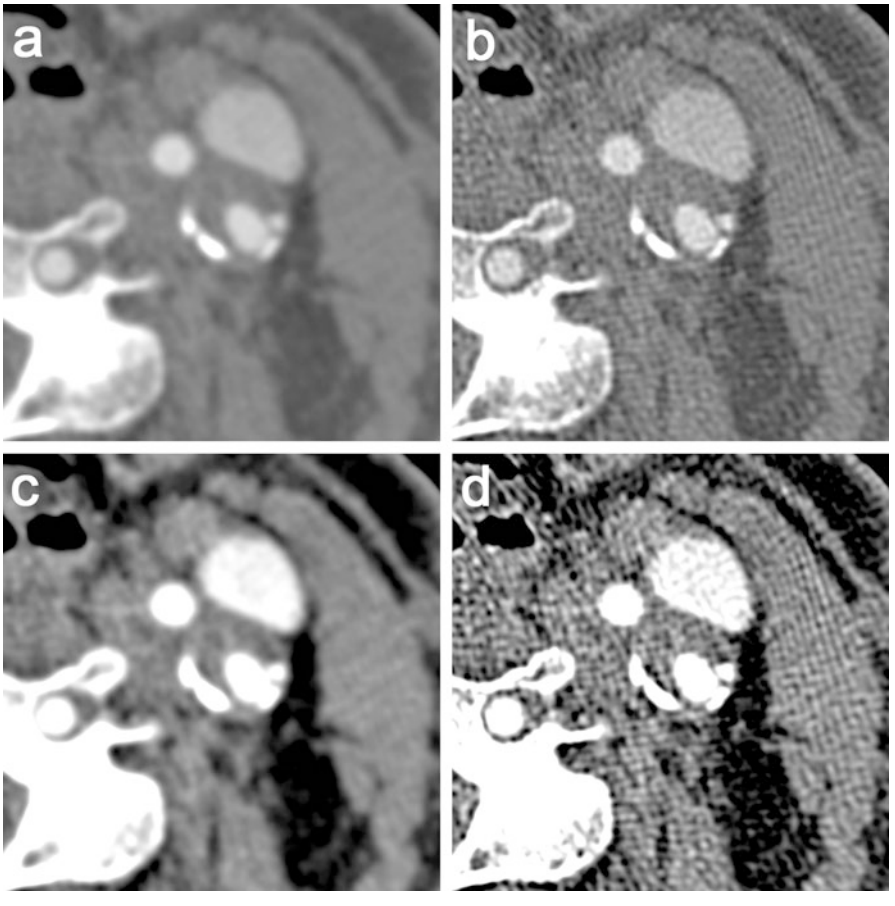

Fig. 11.1 Influence of window-level setting and convolution kernels on the evaluation of lumen and plaque. Four axial MDCT images through the carotid bifurcation obtained with a smooth (**a**, **c**) or a sharp (**b**, **d**) kernel and with a larger (W1000 L200; **a**, **b**) or smaller (W400 L100; **c**, **d**) window width setting. A large window width (**a**, **b**) gives a better differentiation between lumen and neighboring calcifications, which mostly appear brighter. A smaller window width (**c**, **d**) enables visualization of the small density differences inside the non-calcified part of the plaque. A sharper reconstruction kernel (**b**, **d**) increases the contrast between the small dense calcifications and the surrounding structures, whereas a smoother kernel (**a**, **c**) leads to averaging of contrast differences, which gives a smoother appearance to the structures

nal dimensions and therefore the accuracy of the stenosis measurements. The extent of blooming also depends on the convolution kernel chosen in the filtered-back projection algorithm. Sharp convolution kernels increase the contrast of small dense structures as the blurring is reduced, whereas smooth kernels lead to averaging of contrast differences. The signal-to-noise-ratio on the other hand improves when applying a smooth kernel because the image noise is reduced.

The appearance of the lumen–wall interface is influenced by adjustment of the window-level setting. Each lumen contrast opacification has been shown to theoretically have its own optimal window-level setting for which lumen measurements are most accurate [20]. When calcifications border the lumen, the two hyperdense structures may be difficult to differentiate from each other, impeding accurate lumen measurement. Normally, in CTA a large window width (500–1,000 HU) is used, which can be adjusted by the reader dependent on the lumen attenuation and the presence of calcifications near the lumen in order to improve the visual differentiation between dense structures. Figure 11.1 illustrates the influence of window-level setting and convolution kernels on the evaluation of the lumen.

In MDCTA images a challenge is formed by the artifacts from extra luminal dense structures like dental material, bone, and atherosclerotic calcifications which might obscure a clear visualization of the lumen. Correct head positioning with a slight tilt of the head and an upright position of the chin reduces the effect of beam hardening artifacts from dental material at the level of the carotid bifurcation, the predilection place for atherosclerotic disease in the carotid artery (Fig. 11.2). As described, convolution kernels and window-level settings highly influence the appearance of high density structures like calcifications. In addition, with a fixed window-level setting, calcification volumes appear smaller in higher kVp-settings [21].

From the cross-sectional source images, 2D or 3D image reconstructions can be created which aid in the identification and measurement of the maximal stenosis. Multiplanar

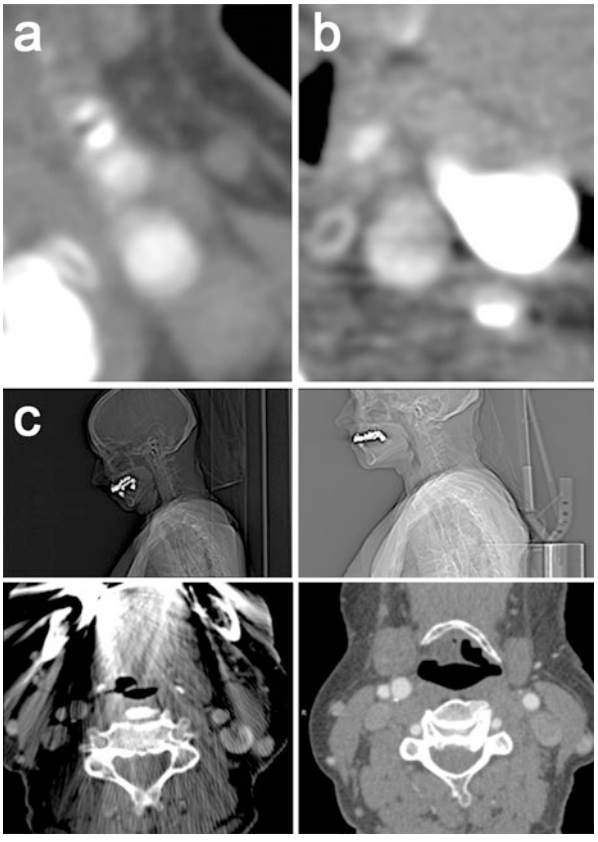

Fig. 11.2 Influence of artifacts on MDCTA imaging. (**a**) Axial image at a level above the carotid bifurcation showing motion artifacts due to swallowing. The tissue boundaries are heavily blurred. (**b**) The dependent part of the jugular vein is filled with high density contrast material, which causes streaks of low attenuation, artificially introducing a low contrast area in the neighboring carotid artery and hampering visualization of its wall. (**c**) Dental material can cause enormous streak artifacts (images on the *left*), impeding correct judgment of surrounding structures. A slight upward tilt of the chin moves these artifacts away from the region of interest and allows a normal visualization of the larger part of the carotid bifurcation (as shown on the *right*)

reconstructions (MPR) and curved planar reconstructions (CPR) provide 2D images of any predefined plane and enable accurate stenosis measurement. For creating a longitudinal view of the artery, CPR has the advantage over MPR that it corrects for vessel curvature outside of the plane. Shaded surface display (SSD), volume rendering (VR), and maximum intensity projection (MIP) are all 3D techniques with their own strengths and weaknesses. In SSD all pixels with densities below a certain threshold are excluded and the remaining data are viewed as if their surfaces are illuminated by a point source. VR utilizes the image intensities directly, by assigning opacity and color coding, to create 3D reconstructions. Both techniques are less useful for carotid artery stenosis measurements. MIPs are created by projection of the maximum intensity pixels from a 3D data set on a predefined 2D plane and give a simple overview of the vessel and its stenosis. However, this technique is limited in arteries with atherosclerotic calcifications, since calcifications in the vessel wall can easily cover the contrasted lumen causing overestimation of the degree of luminal stenosis. In addition, bony structure like the spine, thyroid cartilage, cricoid, and hyoid might interfere with a clear overview of the artery in 3D post-processing techniques (Fig. 11.3).

New techniques have been investigated that might solve the problem of artifacts from bone and calcifications on images. Matched mask bone elimination (MMBE) is a technique for the automated removal of bone pixels from CTA data sets. Preceding to the CT angiography a nonenhanced data set is acquired on which the bone pixels are identified. The corresponding pixels on the registered CT angiography are assigned an arbitrarily low value and MIP images free from overprojecting bone can then be obtained [22, 23]. Whereas for MMBE, acquisition and registration of two separate datasets is necessary, in dual-energy CT (DECT) two image data sets can be simultaneously acquired with different tube voltages (for example 80 and 140 kVp). Tissues can be differentiated by analysis of their attenuation differences depending on the tube voltage. The attenuation difference is especially large in materials with a high atomic number, such as iodine. Bone and calcifications, which show a smaller attenuation difference, can therefore be differentiated from iodine in the carotid lumen. As a result, calcifications can be removed from the contrast-filled lumen, enabling quantification of carotid stenosis in heavily calcified arteries [24]. However, because in both techniques an additional rim around the calcified pixels is removed due to blooming artifacts, overestimation of the grade of stenosis can still be introduced.

2.2 Stenosis Measurement

The accuracy of the stenosis measurement is important, seen its role in clinical decision making about carotid endarterectomy. Traditionally, the stenosis in the carotid artery was assessed using intra-arterial digital subtraction angiography (DSA), which is still considered the gold standard. The degree of stenosis was defined as the residual lumen at the stenosis as a percentage of the normal lumen in the distal internal carotid artery (according to the NASCET criteria) or as the residual lumen as a percentage of the estimated original diameter of the artery at the level of the stenosis (according to the ECST criteria). In the large symptomatic carotid surgery trials, conventional DSA was performed in two or three projections (lateral, posterio-anterior, and/or oblique) which were investigated for the most severe stenosis. Whereas rotational DSA, using multiple planes, showed to provide a benefit in detecting the smallest diameter in a stenosed artery compared to conventional DSA [25], the association

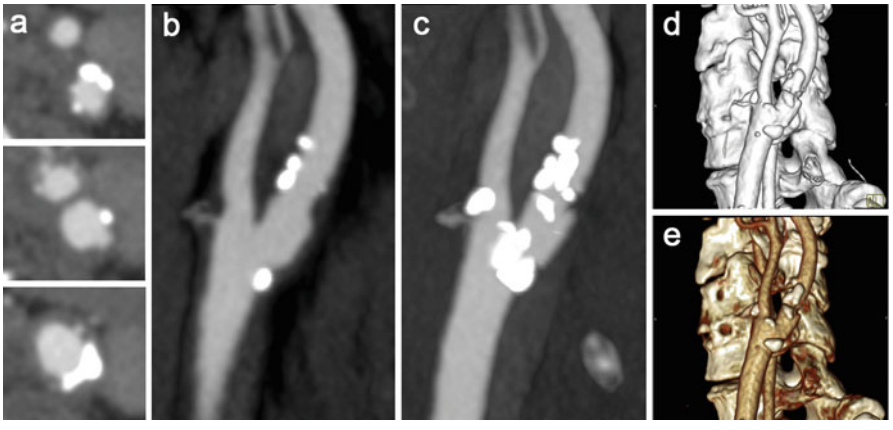

Fig. 11.3 [!t]Different post-processing techniques in MDCTA images of a moderately stenosed carotid artery. (**a**) Axial slices through the common carotid artery (*lower image*), the level of the carotid bifurcation (*middle*), and a level above the bifurcation (*upper image*). (**b**) Multiplanar reformat (MPR) in the sagittal plane visualizing the atherosclerotic plaque around the bifurcation. (**c**) Maximum intensity projection (MIP, 8.8 mm) in the same plane. Over projection of calcifications hampers a clear visualization of the lumen. (**d**) Volume rendering (VR) shows a 3D reconstruction of the carotid artery. (**e**) Shaded surface display (SSD) of the same carotid bifurcation. Both last techniques suffer from over projection of calcifications

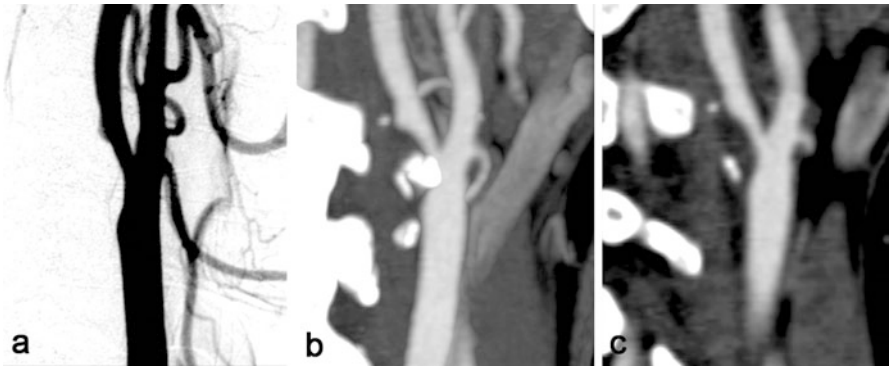

Fig. 11.4 Assessment of carotid stenosis with DSA and MDCT angiography. (**a**) Digital subtraction angiography (DSA) of a right carotid artery shows a 50 % stenosis at the level of the bifurcation. (**b**) A maximum intensity projection (MIP, 6 mm) of MDCTA images of the same artery. MIP has the disadvantage of overprojection of calcifications over the lumen, causing overestimation of stenosis measurement. (**c**) A multiplanar reformatted image (MPR, 1 mm) in the same plane as the MIP in (**b**); the problem of overprojection does not occur here. Using MPR reconstruction of 3D data the point of maximum stenosis can be found easier compared to using DSA

between the severity of stenosis and stroke risk and therefore the indication for surgical intervention remained based on conventional DSA.

The volumetric CTA datasets allow for MPRs and MIPs in any plane and therewith provide much more information on the lumen and its morphology than conventional DSA. The residual lumen is almost never circular and DSA performed in a limited number of projections does not always reveal the narrowest lumen. Analysis of 3D information therefore may provide a more realistic way to assess the true maximum stenosis.

In case CTA replaces DSA in clinical decision making, stenosis measurements on CTA should be performed in a comparable way, i.e., measuring the diameter of the remaining lumen at the level of the maximal stenosis and of the normal lumen distal to the stenosis. This can be done in several ways using different post-processing techniques. Although with MIP reconstructions images comparable to those in DSA can be obtained, this technique is limited in calcified plaques and it is recommended not to use MIP images for stenosis measurements in arteries with calcifications (Fig. 11.4). Generally, one uses 3D software to create MPRs and/or CPRs in oblique planes parallel to the carotid lumen to seek the point of maximum stenosis and measures the smallest diameter in the cross-sectional plane perpendicular to the central lumen line at that level. Figure 11.5 shows this method of stenosis measurement using 3D software. The reference diameter is measured in the same way at a level above the carotid bulb where the lumen walls run parallel to each other (i.e., the healthy distal carotid artery).

When using the ECST criteria to assess the degree of stenosis, CTA directly enables visualization of the outer

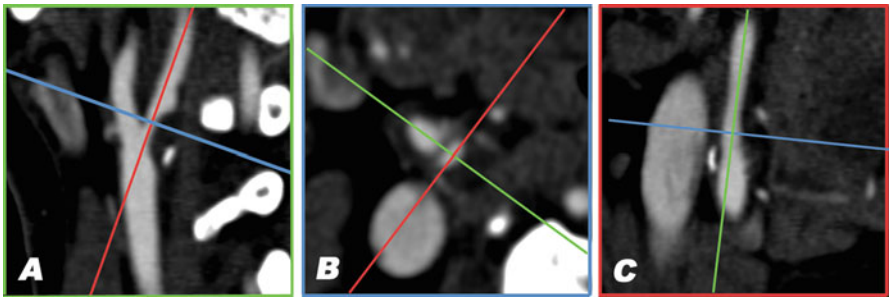

Fig. 11.5 Stenosis measurement in MDCT angiography using 3D software. Multiplanar reformatted images are created in planes parallel and perpendicular to the lumen axis; the smallest lumen diameter in the cross-sectional plane can then be measured using calipers. (**a**) A sagittal view of the carotid bifurcation. The *blue* and *red lines* correspond to the planes that are depicted in **b** and **c**, respectively. A large atherosclerotic plaque is visible at the origin of the internal carotid artery, causing a high-grade stenosis. (**b**) The cross-sectional image perpendicular to the central lumen line at the level of the smallest vessel diameter. The residual lumen has an *oval shape*. (**c**) The view perpendicular to those in **a** and **b**. In this plane the stenosis is not very prominent (Color figure online)

vessel wall, whereas on DSA the vessel diameter has to be estimated by delineating the projected lumen contour. Therewith, CTA takes into account the changes in vessel diameter caused by vascular remodeling, whereas this phenomenon is ignored when measured on DSA. This might cause differences in ECST stenosis measurements between CTA and DSA.

2.3 Diagnostic Accuracy

Several diagnostic studies have been performed which compared single slice CTA with DSA in the assessment of carotid stenosis. From a meta-analysis of studies published between 1990 and 2003, single slice CTA has been shown to have a pooled sensitivity of 85 % and a pooled specificity of 93 % for detection of a 70–99 % stenosis. Sensitivity and specificity for detection of an occlusion were 97 % and 99 %, respectively [26]. Another systemic review reported a pooled sensitivity of 95 % and a specificity of 98 % for the detection of a 70–99 % stenosis [27]. The latter study also found that CTA was sensitive (95 %), but slightly less specific (92 %) in depicting stenosis >30 %. In 2006, Wardlaw and colleagues performed a meta-analysis comparing noninvasive imaging techniques with intra-arterial angiography. They found only 11 studies on CTA, published between 1980 and 2004, that explicitly met the Standards for Reporting of Diagnostic Accuracy (STARD) criteria [28] and they reported a sensitivity of 77 % and a specificity of 95 % for diagnosing 70–99 % stenosis using CTA [29]. The authors warned for the methodological shortcomings of many studies evaluating diagnostic imaging. They concluded that the existing data might support the cautious use of noninvasive imaging to diagnose 70–99 % stenosis, but that more data are needed from carefully designed trials to determine true sensitivity and specificity of noninvasive imaging techniques in routine clinical practice, especially for 50–69 % stenosis, or when used in combination [29]. In 2009, Chappell and colleagues performed an individual patient data meta-analysis to find clinically significant estimates of the accuracy of non-invasive imaging in diagnosing severe and moderate symptomatic artery stenosis [30]. They also concluded that existing primary studies provide limited data and that the literature overestimates the accuracy of noninvasive imaging techniques. The small CTA dataset included in this analysis revealed a sensitivity and specificity of 65 % and 56 % for detection of 70–99 % stenosis, respectively [30].

A difficulty in the evaluation of the accuracy of stenosis measurement using noninvasive imaging techniques is that both acquisition and post-processing procedures evolve rapidly. Although multidetector CTA is now widespread and is expected to improve diagnostic accuracy, this has barely been tested. Only one study compared MDCTA with DSA and found MDCTA to have a high specificity and a high negative predictive value for significant carotid disease [31]. Since DSA is not routinely used anymore in clinical practice, the assessment of new noninvasive imaging techniques against DSA can not be justified ethically anymore. Therefore there is an increasing need for practical, reliable methods for evaluating new technologies, for example, by standardized comparison with other non-invasive tests or test phantoms.

Both aforementioned systemic reviews [26, 27] did not provide enough evidence to draw robust conclusions about the diagnostic accuracy of the different post-processing techniques, although stenosis assessment using axial slices and MIPs seemed to be better than when using VR and SSD [27]. Most studies did not report on the exact—combinations of—reformatting techniques used, which hampers a solid meta-analysis. More recent studies comparing the post-processing techniques in MDCTA revealed that stenosis measurements on axial source images are highly reproducible and accurate and that the additional use of MPRs or other reconstructions

is not necessary, but might aid in finding the location of the maximum stenosis [32–34].

2.4 (Semi)automated Quantification of Luminal Measures

Manual lumen segmentation and stenosis quantification are laborious and suffer from interobserver and intraobserver variability. Consequently much work has been performed on the development of (semi)automated lumen quantification. The majority of publications with respect to lumen quantification focus on the segmentation of the lumen while the assessment of the severity of luminal stenosis is addressed by few.

Lumen segmentation methods have been reviewed and grouped according to the mathematical framework used [35] or categorized with respect to (1) the way vessel geometry and appearance are modeled, (2) the image features which are used for vessel extraction, and (3) the methodology used in vessel extraction [36].

Some of the published methods have been tailored to or evaluated on carotid CTA images [37–40]. Reported values vary highly. However the comparison of these methods is hampered by the fact that they all use different imaging data and evaluation measures, like Dice similarity coefficient, mean surface distances, or visual inspection. In addition, most studies were performed on small and selected data sets. Figure 11.6 illustrates a 3D lumen segmentation of a carotid bifurcation.

To facilitate an objective comparison of carotid artery segmentation and stenosis quantification algorithms, the Carotid Bifurcation Algorithm Evaluation Framework was set up in 2009 (http://cls2009.bigr.nl/) [41]. This framework consists of a publically available image database, annotated data for training and evaluation, and standardized evaluation measures. Till date nine algorithms have been evaluated by the framework, of which only one is fully automatic, whereas the others require three initialization points. The three best performing methods evaluated by the framework have dice similarity coefficients of 0.92, 0.88, and 0.90, mean surface distances of 0.18, 0.54, and 0.17 mm and Hausdorff distances of 1.5, 4.4, and 1.7 mm, respectively [41]. Figure 11.7 shows three examples of lumen segmentations with three different dice values.

These three best performing methods are based on three different approaches, i.e., graph cut, level set, and active surface algorithms [41].

In the graph cut framework voxels are assigned to vessel lumen or background by considering all image voxels as nodes in a three-dimensional graph and creating an optimal surface which separates (cuts) the foreground (lumen) from the background. To compute this optimal cut the image gradient can be used.

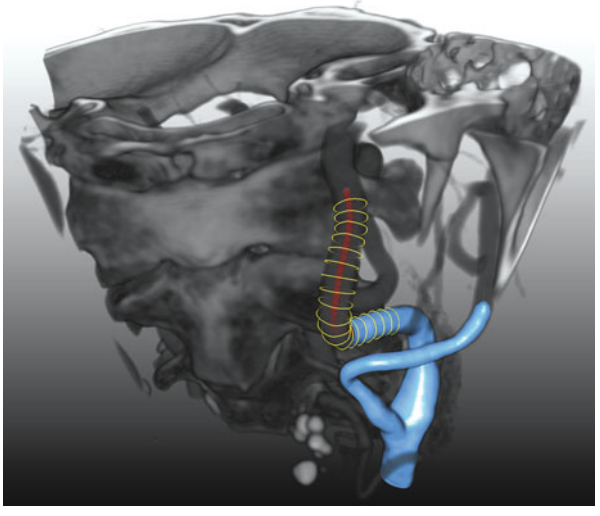

Fig. 11.6 3D-segmentation of the lumen of a carotid artery. An example is shown of a carotid artery lumen segmentation using three different segmentation representations. The *red dots* indicate a centerline through the centroids of the vessel cross sections. The *yellow* "*circles*" show the lumen contours perpendicular to the centerline. The *blue* surface shows an interpolated surface through the *yellow* contours (Color figure online)

In the level set framework, the vessel surface is represented implicitly by the zero level lines (zero level set) of an embedding function (similar as, e.g., sea level in a height map). This embedding function is then changed (evolved), implicitly resulting in deformation of the zero level set. This representation has the advantage that the zero level set can change topology (Fig. 11.8). The evolution of the embedding function should ensure that the zero level set halts at the vessel lumen boundary. This is achieved by defining a speed function derived from the image data. Both the initial segmentation and the design of the speed image are the key ingredients in the design of a level set-based segmentation method.

Active surfaces are a generalization of active contours (also called snakes). Using active surfaces the segmentation is also the result of the evolution of an initially segmented surface. However changing topology is much harder to model in this framework. The segmentation is modeled as a surface on which forces are acting which causes the evolution of the segmentation. This evolution can be constrained by properties of the used surface representation.

Although considerable research has been performed on vessel lumen segmentation, only few researchers have published on automatic vessel stenosis grading [42–44]. Also, approaches differ widely in the evaluation that has been performed, both with respect to evaluation measures and number of data sets used.

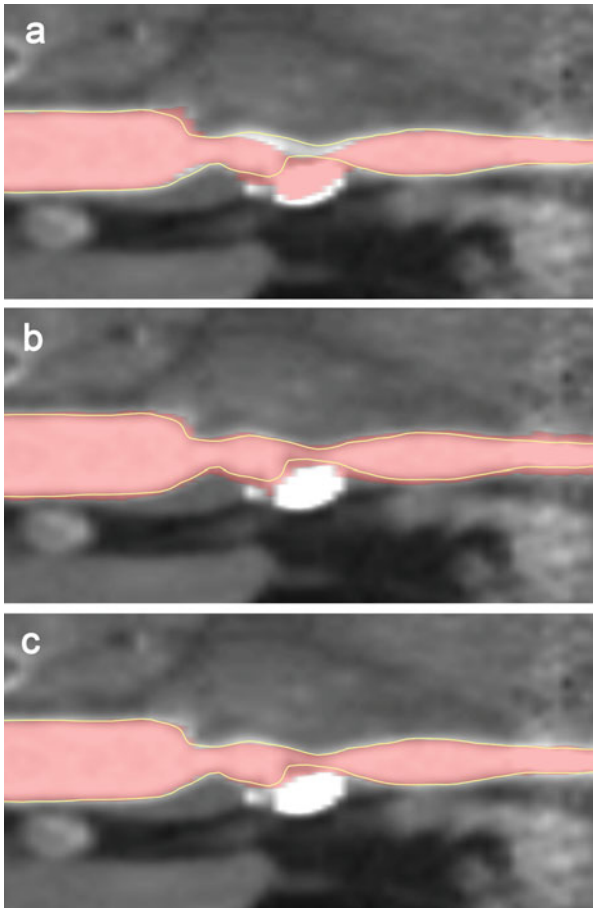

Fig. 11.7 (Semi)automated lumen segmentations of a carotid artery of different qualities. Shown are curved multiplanar reformats (CMPR) of a carotid artery with a calcified atherosclerotic plaque that causes a high-grade stenosis. A visual impression is shown of the reference standard (*yellow line*) based on manual annotations by three observers and automated lumen segmentations (in *red*) that have different qualities: (**a**) with a bad Dice similarity index (SI) of 0.881, (**b**) a moderate Dice SI of 0.884 and (**c**) a good Dice SI of 0.945. The Dice similarity indices are calculated on the whole volume of which the shown CMPR is just a single plane (Color figure online)

The evaluation framework discussed previously also allows objective comparison of performance in stenosis quantification. To date only three stenosis grading methods have been evaluated using this framework, also indicating that this field has received less attention [41]. Clinically, the minimal diameter is often used to calculate the stenosis degree. However, the minimal diameter of a non-elliptical shape is not uniquely defined and is therefore prone to measurement errors and is hard to measure automatically. The evaluation framework evaluates two stenosis measures: an area-based measure which compares the area of the lumen at the stenosis to the area of a distal vessel part and a measure that compares the minimal diameter at the two positions. In the framework, the diameter-based stenosis degree is defined by the smallest line that divides the cross-sectional area in two equal parts. Using automated lumen segmentation, the minimal diameter can easily be replaced by the lumen cross-sectional area. This is a much more accurate measure for the obstruction of the blood flow as carotid arteries, especially at the site of atherosclerotic plaque, generally do not have circular luminal cross sections and also do not run exactly perpendicular to the axial plane of the CT scan. Zhang et al. investigated the use of area measurements and found that assessment of area stenosis on CTA was highly reproducible and showed a satisfactory agreement with diameter stenosis on DSA, although it provides a less-severe estimate of the degree of carotid stenosis, especially in noncircular lumens [45]. The average error in assessing carotid artery stenosis of the best stenosis grading method according to the evaluation framework was 16.9 % for area-based and 17.0 % for diameter-based measurements [41].

Besides stenosis grading, lumen segmentation also enables the extraction of other quantitative measures. The extracted lumen model can, e.g., be used for Computation Fluid Dynamic calculations to assess the shear stress in the atherosclerotic carotid bifurcation [46] and the quantification of geometric parameters such as vessel tortuosity and bifurcation angles [47].

3 Plaque Imaging Using CTA

3.1 Technical Aspects

Assessment of different atherosclerotic plaque components in CTA relies on the differences in linear attenuation coefficient expressed in Hounsfield Units (HU) of the plaque components. Plaque component differentiation is highly dependent on scan parameters.

Reconstruction of thin slices is very important for plaque evaluation. Thin slices allow for datasets with isotropic and higher resolution and therefore enhance the differentiation of plaque components. Especially for plaque components of which HU values are close, like lipid and fibrous tissue, thin slices are crucial.

Where blooming artifacts from vessel wall calcifications can hamper correct stenosis measurements, it also causes a problem in the evaluation of plaque, since it interferes with optimal plaque characterization of the non-calcified part of the plaque. The finite spatial resolution of CT causes partial volume averaging and therefore blooming artifacts. Blooming of calcifications leads to overestimation of calcification size and inability to evaluate the atherosclerotic regions that border the calcifications. Moreover, the calcification volume appears larger when using lower kVp settings [21].

For accurate differentiation of plaque components a high signal-to-noise ratio (SNR) is necessary. Image noise depends mainly on the product of the tube current and rotation

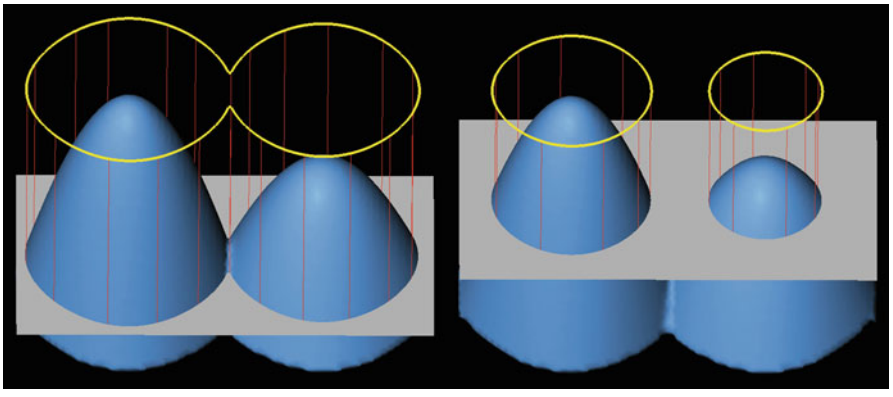

Fig. 11.8 Level set method for lumen segmentation. Using the level set framework a segmentation (indicated by the *yellow contours*) is seen as the zero level (*gray plane*) of an embedding function in a higher dimension (*blue surface*). If the embedding function changes as is indicated by the two *blue* surfaces which are slightly different, the zero level (segmentation) changes. Using this framework a segmentation can easily change topology. The segmentation on the *left* has one object (*contour*) while the segmentation on the *right* consists of two distinct objects (Color figure online)

time (mAs), the tube voltage, and reconstruction kernel. Because the atherosclerotic plaque is a relative small structure, a thin slice thickness and a small field-of-view are required. These result in a decrease of SNR, which should be compensated by a higher radiation exposure.

High intraluminal contrast material density may influence the density measurements in the plaque. Ex vivo studies in coronary arteries revealed that intraluminal attenuation strongly affects the measured attenuation of the plaque [48]. This can be explained not only by partial volume effects but also by the entrance of contrast material in the plaque via the vaso vasorum. It is unknown yet if this effect is also seen in the larger carotid artery, but it underlines the necessity of standardized scan protocols, especially since carotid plaque enhancement in CTA is thought to be associated with increased risk for neurological events [49, 50].

Another technical aspect influencing accurate differentiation of plaque components in CTA is the convolution kernel used for reconstruction of the image dataset. The convolution kernels allow for influencing the image characteristics; a smooth algorithm will reduce spatial resolution, image noise, and image contrast for tiny structures, whereas a sharp algorithm has the opposite effect. Plaque characterization and quantification of the different plaque components based on measurement of HU densities is thus highly influenced by the convolution kernel used. Smooth kernels hamper the correct differentiation between tissues with small differences in density, as is the case for lipid and fibrous tissue. In contrast, sharp kernels not only increase contrast differentiation but also lead to an increase in calcium size and low-intensity rings around calcifications (edge-enhancement artifacts), which hamper further plaque interpretation. Intermediate reconstruction kernels turned out to allow optimal plaque interpretation [21].

The window-level setting also influences the visualization of the different plaque components. Whereas a large window-width is used in luminography to differentiate lumen from calcifications that border the lumen, a small window-width is necessary to enhance the small differences in HU density inside the non-calcified plaque (Fig. 11.1).

3.2 Diagnostic Accuracy

3.2.1 Plaque Surface Morphology

The accuracy of DSA in the detection of plaque ulceration, as compared to macroscopic surgical observations, has been found to be low (sensitivity 46 % and sensitivity 74 %) [51]. CTA allows for analysis of the plaque surface (Fig. 11.9) and the differentiation between ulcerations and irregularities and has been demonstrated to perform better than DSA [52]. A validation study, comparing single slice CTA with histological specimens reported a sensitivity and specificity of 60 % and 74 %, respectively [53]. However, MDCTA has been found to have a high sensitivity and specificity (94 % and 99 %, respectively) in detecting plaque ulcerations compared to surgical observation [54]. Assessment of plaque ulceration on MDCTA is highly reproducible ($\kappa > 0.86$) [55, 56].

3.2.2 Plaque Composition

The first validation studies compared 3 mm single slice CT images with histological sections from carotid endarterectomy specimens and did not show clear-cut results. Whereas two studies reported that calcifications, lipid, and fibrous tissue could be differentiated based on density measurements [57, 58], another study concluded that single slice CT was not sufficiently robust to reliably characterize plaque composition and plaque morphology [53]. The introduction of multidetector CT enabled a more detailed analysis of the

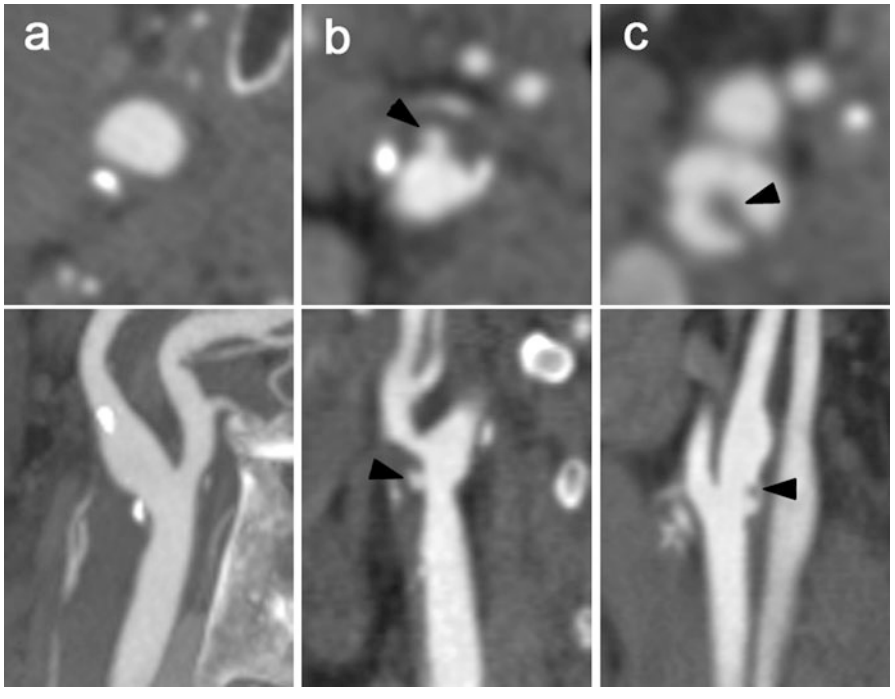

Fig. 11.9 Assessment of plaque surface morphology using MDCT angiography. Cross-sectional images (*upper panels*) perpendicular to the central lumen line and multiplanar reformats (*lower panels*) of carotid bifurcations. (**a**) An atherosclerotic carotid plaque with a smooth surface. (**b**) A plaque at the level of the carotid bifurcation with an ulceration (*arrowhead*). (**c**) An ulcerated plaque with thrombus material (*arrow head*) that protrudes into the lumen

atherosclerotic carotid plaque composition and the differentiation of plaque components.

Several validation studies have been performed, in carotid arteries as well as in coronary arteries. In coronary artery studies, intravascular ultrasound (IVUS) is used as a gold standard. In carotid artery studies, the availability of histological carotid plaque specimens from carotid endarterectomy enables reliable validation against histology. An additional advantage is that the characterization of the separate plaque components can be performed easier and in more detail in the larger carotid arteries. In 2005, we performed an ex vivo validation study, in which CEA specimens were scanned and the images were compared with the histological slices (Fig. 11.10). The CT value of lipid-rich regions differed significantly from that of fibrous-rich regions (45 ± 21 HU versus 79 ± 20 HU, $p < 0.001$). An ROC analysis revealed 60 HU as the optimal cut-off point for differentiation between lipid and fibrous tissue, with a sensitivity of 89 % and a specificity of 93 % [21]. The study was repeated in vivo, in which the CT values for lipid- and fibrous-rich tissue were 25 ± 19 HU and 88 ± 18 HU, respectively. Again an optimal threshold value of 60 HU was found, with a sensitivity and specificity of both 100 % [59]. Calcifications are easily detected on CT images as high density structures and equivalent to coronary calcium scoring in electron beam CT, 130 HU is generally taken as a threshold for differentiating calcifications.

Wintermark and colleagues performed a validation study in which they compared in vivo MDCTA images with histological sections for the non-calcified plaque components and with ex vivo MDCTA images for the calcifications [56]. They found the following scan-parameter dependent cut-off values, determined as the half way HU attenuation value between the average HU values of each plaque component: 39.5 HU between lipid-rich necrotic core and connective tissue, 72.0 HU between connective tissue and hemorrhage, and 177.1 HU between hemorrhage and calcifications. They further compared the CT classification with the histological classification of type of atherosclerotic plaque and stage of lesion development according to the system derived from the AHA classification and found an overall agreement of 72.6 % (unweighted κ of 67.6 %) [56]. The concordance for calcifications was perfect, whereas the reliability of the identification of the non-calcified plaque components was limited due to overlap of the values between the soft components. However, CTA showed good correlation with histology for larger lipid cores and larger hemorrhages. Further they demonstrated that CTA performed well in measuring fibrous cap thickness ($R^2 = 0.77$, $p < 0.001$) [56].

3.3 Quantification of Plaque Components

Calcifications in the vessel wall can easily be measured in a quantitative way. Agatston and colleagues were the first to quantify coronary calcifications with electron beam CT [60]. As a default, the threshold to differentiate calcification is $\geq$130 HU in non-contrast CT scans. Although the Agatston score as a quantification tool can be used in carotid arteries, other scoring methods like a volume score are more frequently used [61]. However, when CTA images are used, the threshold has to be higher in order to automatically

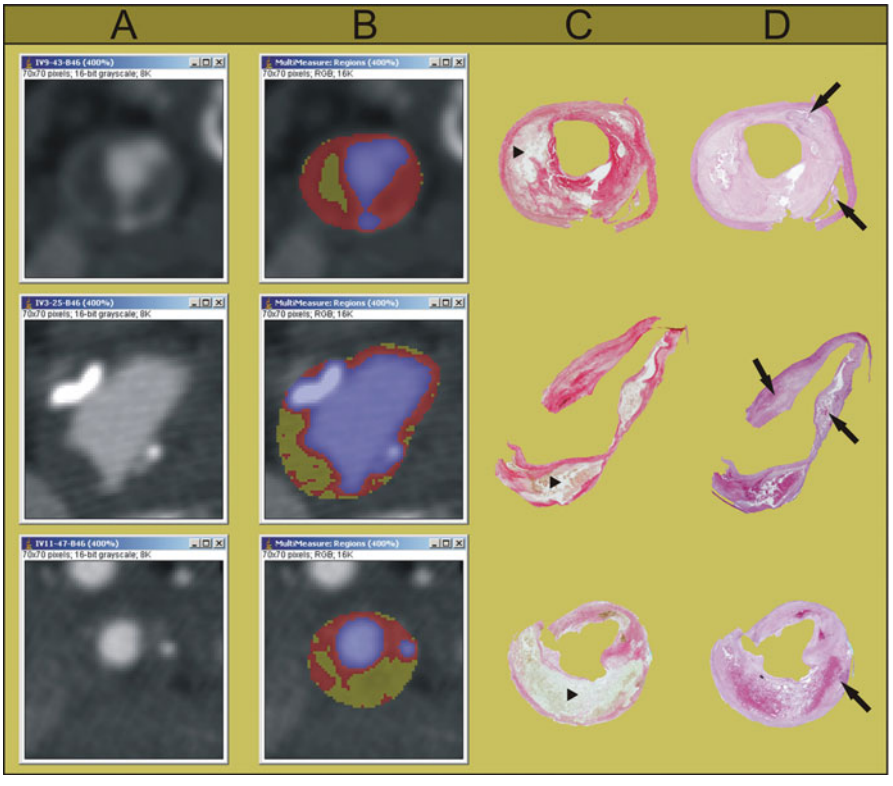

Fig. 11.10 Hounsfield attenuation-based differentiation of plaque components—validation against histological sections. Column **a**: axial MDCT images of a carotid artery with atherosclerotic plaque. Column **b**: MDCT plaque composition based on HU differences. Column **c**, **d**: Corresponding histological sections with Sirius Red (SR) and hematoxylin eosin (HE) staining, respectively. *Blue* regions in the MDCT plaque composition images correspond well with lumen and calcifications on HE stained histological sections (*arrows*). The *red* regions correspond well with the *red* collagen-rich regions in the SR stained sections. *Yellow* regions correspond with the lipid core (i.e., lipid, hemorrhage, and necrotic debris) (*arrowhead*) regions on histology (the *non-red* regions on the SR stained sections that are not calcified areas on the HE stained sections). (Reprinted with permission from de Weert TT, Ouhlous M, Meijering E, et al (2006) In vivo characterization and quantification of atherosclerotic carotid plaque components with multidetector computed tomography and histopathological correlation. Arterioscler Thromb Vasc Biol 26(10):2366–2372) (Color figure online)

differentiate calcifications from the bordering luminal contrast. Another possibility is to first delineate the inner and outer borders of the carotid plaque and subsequently discriminate calcifications using a threshold of 130 HU within the plaque. In this way, 3D volumetric MDCTA datasets also allow for quantification of the soft plaque components.

Annotation of the luminal area can be done (semi)automatically based on thresholds that separate the bright, contrast-filled lumen from the lower density plaque. However, calcifications bordering the lumen might be included in the lumen segmentation and therefore manual correction is necessary. Using lumen and outer vessel wall contours, the plaque area can be calculated by subtracting lumen area from total vessel area.

Validation studies of plaque area measurements with histology as gold standard are hampered by the fact that histological preparation leads to shrinkage of the specimens. Nevertheless, strong correlations have been found between ex vivo and in vivo MDCTA and histology for the assessment of plaque area ($R^2 = 0.81$ and 0.73, respectively) [21, 59]. Intraobserver reproducibility of plaque area measurements with MDCTA was good (coefficient of variation of 8 %) [59].

The CT value thresholds in HU that differentiate between plaque components create the opportunity to quantify plaque composition. The aforementioned in vivo validation study, comparing MDCTA images with histological specimens, showed that area measurements of calcifications were overestimated by MDCTA; however the correlation with histology was good ($R^2 = 0.74$). The correlation between MDCTA and histology for fibrous area measurements was also good ($R^2 = 0.76$) but was poor for lipid ($R^2 = 0.24$). Further investigation, however, showed that this correlation improved in mildly calcified plaques and non-calcified plaques ($R^2 = 0.77$ and 0.81, respectively). The intraobserver variability of area measurements of the different plaque components was low, with a coefficient of variation of 8 %, 11 %, and 15 % for calcifications, fibrous tissue, and lipid, respectively [59].

Plaque volume and plaque component volumes can be calculated by multiplying area measurements with slice increment and the number of slices in the range of interest.

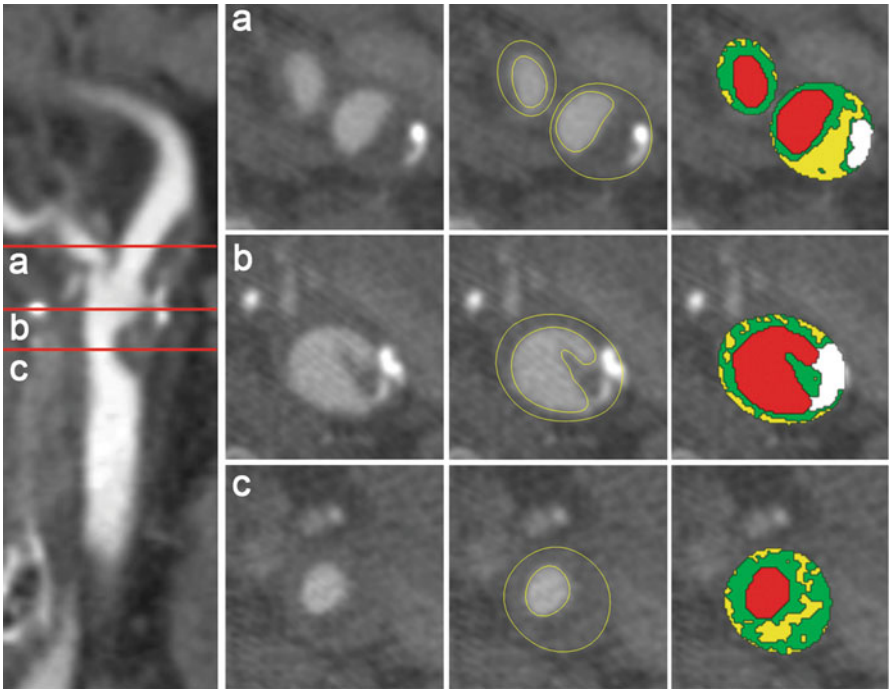

Fig. 11.11 (Semi)automated segmentation of lumen and plaque components. (Semi)automated segmentation of lumen and plaque is performed on axial images within a predefined range. Contours of lumen and plaque are generated and can be manually adjusted if necessary. Within the plaque area (outer vessel wall contour minus lumen contour) the plaque components are differentiated based on Hounsfield Unit thresholds (lipids: <60 HU, fibrous 60–130 HU, calcification >130 HU). The *color overlay* shows the different structures; lumen = *red*, lipid = *yellow*, fibrous = *green*, calcification = *white*. This figure shows a CPR image of a carotid bifurcation on the *left* and plaque segmentation on axial slices at three levels: (**a**) through the internal and external carotid artery, showing a large, mainly non-calcified atherosclerotic plaque in the internal carotid artery; (**b**) through the distal common carotid artery just below the bifurcation on which an ulcerated surface is visible; and (**c**) through the common carotid artery at the level of the smallest vessel diameter (Color figure online)

In an in vivo study in 56 patients, plaque volume and plaque component volumes could be assessed in a reproducible way. The difficulty of defining the transition of normal wall into atherosclerotic plaque contributes highly to the interobserver variability. Consensus about the longitudinal dimensions of the plaque improved the reproducibility of plaque volumes strongly [62].

3.4 (Semi)automated Plaque Measurements

Manually assessing lumen and vessel contours is a time-consuming task and is highly influenced by the window-level setting. Segmentation of the outer vessel wall and subsequent automated plaque characterization has received considerably less attention than luminal analysis.

The challenge of automated analysis of carotid atherosclerotic plaque lies in the difficulty of defining the outer vessel wall. This is a challenging task due to the low and varying contrast between the plaque and its surrounding soft tissue. Vukadinovic et al. developed a semiautomated method to segment the outer vessel wall [63], which only required clicking initialization points for lumen segmentation and clicking seed points for defining the range of interest for plaque segmentation. The method uses a level-set framework for vessel lumen segmentation [37], followed by classification of calcium objects using a set of image features related to the appearance, shape, and size of bright objects in the CTA data set. Subsequently, image voxels are identified as lying inside or outside the vessel wall, using a same set of image features. Finally, the outer vessel wall is determined by fitting an ellipsoid that utilizes the information from the calcium and inner/outer vessel classification step. After generation of the inner and outer vessel wall contours, the plaque components (lipid, fibrous tissues, and calcifications) are automatically differentiated based on the aforementioned HU-thresholds. Figure 11.11 shows the results of (semi)automatically generated plaque segmentations.

The method has been trained and tested on manually annotated MDCTA datasets of the carotid arteries and validated against manually segmented carotid arteries. The average Dice similarity index was 91 %, which was comparable to the similarity index between two observers [63]. Subsequently, the performance of this plaque segmentation method in quantifying plaque volume and plaque component

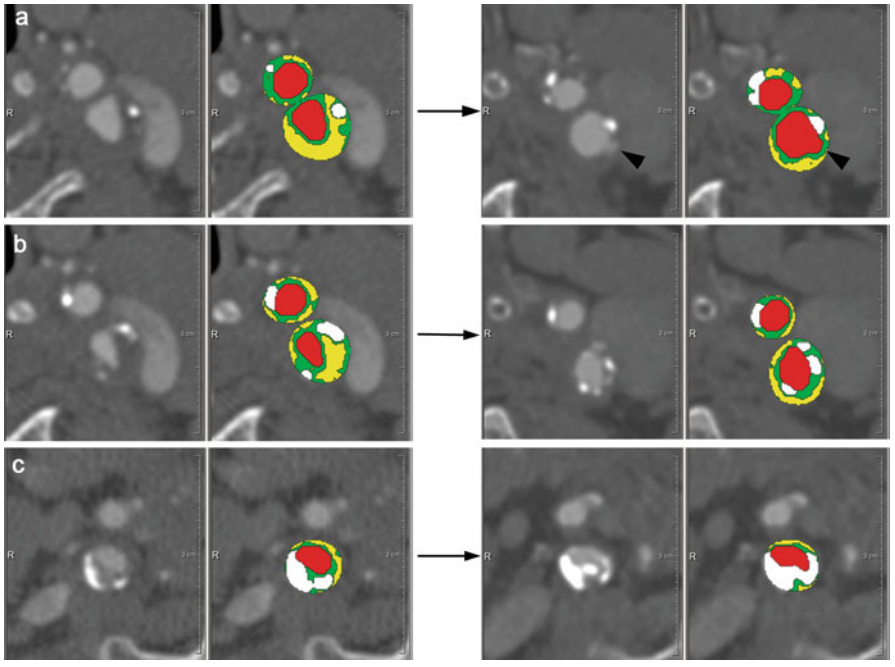

Fig. 11.12 Serial quantitative plaque imaging. Serial plaque imaging in a 67-year-old male patient (**a**, **b**) and a 62-year-old male patient (**c**). On the *left*, axial MDCTA images and the *plaque color overlays* of the baseline scan and on the *right* the corresponding images of the follow-up scan. (**a**) Predominantly non-calcified plaque at a level just above the bifurcation. At follow-up imaging after 6 years an ulceration is visible (*arrow head*). (**b**) Images from the same artery at a more distal site. (**a**, **b**) At follow-up a decrease in plaque volume and a change in plaque composition is demonstrated. (**c**) Internal carotid artery demonstrating an increase in calcification of the vessel wall at follow-up (after 6 years) (Color figure online)

volumes was studied by comparing measurement error of the automated method using manual contours as a reference standard with the interobserver variability in manual annotations. The differences between the automated method and the manual observers were comparable to the interobserver differences [64].

Although the method is highly automated some observer interventions are still needed and the outer vessel wall segmentations should still be checked manually for erroneous in or exclusion of calcifications, and therewith over-segmentation or under-segmentation of the plaque. Taken these manual interventions into account, the intraobserver and interobserver reproducibility of the semiautomated method is better as compared to the reproducibility of manual annotating, with intraclass correlation coefficients of 0.93/0.84 for plaque volume and 0.86–1.00/0.76–0.99 for plaque component volumes (unpublished data).

4 Applications of Quantitative Atherosclerotic Measures

MDCTA-based quantitative plaque measures have been used in several studies to investigate atherosclerotic development. Rozie et al. investigated in a cross-sectional study the correlation between cardiovascular risk factors and plaque volume and plaque composition. They found that plaque volume and severity of stenosis were just moderately correlated, which means that plaque volume could be an additional predictor for ischemic stroke. An increasing plaque volume was associated with increased lipid and calcium proportion and a decreased fibrous proportion. Age and smoking were independently related to plaque volume. Patients with hypercholesterolemia had a significantly higher contribution of calcifications and a significantly lower contribution of lipid in the atherosclerotic plaque [65]. Another study investigated whether plaque features could be correlated with the presence of ulcerations, which is thought to be a marker of plaque rupture [10]. It was demonstrated that degree of stenosis, plaque volume, and the proportion of lipid-rich necrotic-core were associated with the presence of carotid plaque ulcerations [66]. In another cross-sectional study, carotid atherosclerotic plaque features were identified that were significantly different in acute carotid stroke patients compared to non-stroke patients and on the infarct side compared to the contralateral side in stroke patients. These features included increased vessel wall, thinner fibrous caps, greater number of lipid cores, and their location closer to the lumen. The number of calcium clusters was a protective factor [67].

Numerous studies report on the role of plaque calcifications in plaque stability. The findings are not conclusive. A recent systemic review suggests that clinically symptomatic plaques have a lower degree of calcifications than asymptomatic plaques [61]. The percentage calcification within a plaque of a stenosed artery, rather than the absolute volume seems to be associated with plaque stability [68]. This underscores why the (automated) quantification of the relative contribution of the plaque components might add to the improvement of stroke risk prediction.

The MDCTA plaque imaging studies performed so far had a cross-sectional study design. The ability to quantify atherosclerotic features in vivo creates the potential to further explore atherosclerotic plaque development by prospective, serial in vivo imaging of the carotid plaque (Fig. 11.12). Currently, a prospective serial MDCTA plaque imaging study is being performed, which investigates the temporal changes in plaque burden and plaque composition and its determinants in TIA and stroke patients.

5 Summary and Future Directions

Currently, MDCTA is a noninvasive imaging technique frequently used in clinical practice for the assessment of carotid stenosis grading and is replacing the more invasive technique of DSA. MDCTA can perfectly be combined with a native CT scan and a perfusion CT scan of the brain in the evaluation of stroke patients.

Although plaque imaging is currently only used in research settings, the same MDCTA data set might provide further clinically important information on the atherosclerotic plaque burden, plaque surface morphology, and plaque composition for a more individualized risk prediction. Large, prospective studies demonstrating significant associations between CTA-based risk factors and (recurrent) events are yet lacking. Future research should focus on the role of plaque measures in stroke risk prediction and on the use of MDCTA-based quantified plaque measurements in monitoring efficacy of medical therapy. Large—preferably multicenter—studies should pay attention to the standardization of data acquisition and postprocessing across centers and imaging time points, since several technical parameters highly influence quantification of plaque features as is broadly depicted in this chapter. More effort should further be put in the development of robust, accurate, automated quantification of plaque measures in order to minimize measurement variability.

References

1. Roger VL, Go AS, Lloyd-Jones DM, Adams RJ, Berry JD, Brown TM, Carnethon MR, Dai S, de Simone G, Ford ES, Fox CS, Fullerton HJ, Gillespie C, Greenlund KJ, Hailpern SM, Heit JA, Ho PM, Howard VJ, Kissela BM, Kittner SJ, Lackland DT, Lichtman JH, Lisabeth LD, Makuc DM, Marcus GM, Marelli A, Matchar DB, McDermott MM, Meigs JB, Moy CS, Mozaffarian D, Mussolino ME, Nichol G, Paynter NP, Rosamond WD, Sorlie PD, Stafford RS, Turan TN, Turner MB, Wong ND, Wylie-Rosett J, American Heart Association Statistics Committee and Stroke Statistics Subcommittee (2011) Heart disease and stroke statistics – 2011 update: a report from the American Heart Association. Circulation 123(4):e18–e209. doi:10.1161/CIR.0b013e3182009701, CIR.0b013e3182009701 [pii]
2. Warlow C, Sudlow C, Dennis M, Wardlaw J, Sandercock P (2003) Stroke. Lancet 362(9391):1211–1224. doi:10.1016/S0140-6736(03)14544-8, S0140-6736(03)14544-8 [pii]
3. (1991) Beneficial effect of carotid endarterectomy in symptomatic patients with high-grade carotid stenosis. North American Symptomatic Carotid Endarterectomy Trial Collaborators. N Engl J Med 325(7):445–453. doi:10.1056/NEJM199108153250701
4. (1998) Randomised trial of endarterectomy for recently symptomatic carotid stenosis: final results of the MRC European Carotid Surgery Trial (ECST). Lancet 351(9113):1379–1387. doi:S0140673697092921 [pii]
5. Rothwell PM, Eliasziw M, Gutnikov SA, Fox AJ, Taylor DW, Mayberg MR, Warlow CP, Barnett HJ, Carotid Endarterectomy Trialists C (2003) Analysis of pooled data from the randomised controlled trials of endarterectomy for symptomatic carotid stenosis. Lancet 361(9352):107–116, doi:S0140673603122283 [pii]
6. (1995) Endarterectomy for asymptomatic carotid artery stenosis. Executive Committee for the Asymptomatic Carotid Atherosclerosis Study. JAMA 273(18):1421–1428
7. Halliday A, Mansfield A, Marro J, Peto C, Peto R, Potter J, Thomas D, Group MRCACSTC (2004) Prevention of disabling and fatal strokes by successful carotid endarterectomy in patients without recent neurological symptoms: randomised controlled trial. Lancet 363(9420):1491–1502. doi:10.1016/S0140-6736(04)16146-1, S0140673604161461 [pii]
8. Hobson RW 2nd, Weiss DG, Fields WS, Goldstone J, Moore WS, Towne JB, Wright CB (1993) Efficacy of carotid endarterectomy for asymptomatic carotid stenosis. The Veterans Affairs Cooperative Study Group. N Engl J Med 328(4):221–227. doi:10.1056/NEJM199301283280401
9. Naghavi M, Libby P, Falk E, Casscells SW, Litovsky S, Rumberger J, Badimon JJ, Stefanadis C, Moreno P, Pasterkamp G, Fayad Z, Stone PH, Waxman S, Raggi P, Madjid M, Zarrabi A, Burke A, Yuan C, Fitzgerald PJ, Siscovick DS, de Korte CL, Aikawa M, Juhani Airaksinen KE, Assmann G, Becker CR, Chesebro JH, Farb A, Galis ZS, Jackson C, Jang IK, Koenig W, Lodder RA, March K, Demirovic J, Navab M, Priori SG, Rekhter MD, Bahr R, Grundy SM, Mehran R, Colombo A, Boerwinkle E, Ballantyne C, Insull W Jr, Schwartz RS, Vogel R, Serruys PW, Hansson GK, Faxon DP, Kaul S, Drexler H, Greenland P, Muller JE, Virmani R, Ridker PM, Zipes DP, Shah PK, Willerson JT (2003) From vulnerable plaque to vulnerable patient: a call for new definitions and risk assessment strategies: part I. Circulation 108(14):1664–1672. doi:10.1161/01.CIR.0000087480.94275.97 , 108/14/1664 [pii]
10. Lovett JK, Gallagher PJ, Hands LJ, Walton J, Rothwell PM (2004) Histological correlates of carotid plaque surface morphology on lumen contrast imaging. Circulation 110(15):2190–2197. doi:10.1161/01.CIR.0000144307.82502.32, 01.CIR.0000144307.82502.32 [pii]
11. Eliasziw M, Streifler JY, Fox AJ, Hachinski VC, Ferguson GG, Barnett HJ (1994) Significance of plaque ulceration in symptomatic patients with high-grade carotid stenosis. North American Symptomatic Carotid Endarterectomy Trial. Stroke 25(2):304–308
12. Rothwell PM, Gibson R, Warlow CP (2000) Interrelation between plaque surface morphology and degree of stenosis on carotid angiograms and the risk of ischemic stroke in patients with symptomatic carotid stenosis. On behalf of the European Carotid Surgery Trialists' Collaborative Group. Stroke 31(3):615–621
13. Hankey GJ, Warlow CP, Molyneux AJ (1990) Complications of cerebral angiography for patients with mild carotid territory ischaemia being considered for carotid endarterectomy. J Neurol Neurosurg Psychiatry 53(7):542–548
14. Willinsky RA, Taylor SM, TerBrugge K, Farb RI, Tomlinson G, Montanera W (2003) Neurologic complications of cerebral angiography: prospective analysis of 2,899 procedures and re-

view of the literature. Radiology 227(2):522–528. doi:10.1148/radiol.2272012071, 2272012071 [pii]
15. Saba L, Anzidei M, Sanfilippo R, Montisci R, Lucatelli P, Catalano C, Passariello R, Mallarini G (2011) Imaging of the carotid artery. Atherosclerosis 220(2):294–309. doi:10.1016/j.atherosclerosis.2011.08.048, S0021-9150(11)00852-5 [pii]
16. European Society of Radiology (2010) White paper on imaging biomarkers. Insights Imaging 1:42–45. doi:10.1007/s13244-010-0025-8
17. Beitzke D, Wolf F, Edelhauser G, Plank C, Schernthaner R, Weber M, Nolz R, Lammer J, Loewe C (2011) Computed tomography angiography of the carotid arteries at low kV settings: a prospective randomised trial assessing radiation dose and diagnostic confidence. Eur Radiol 21(11):2434–2444. doi:10.1007/s00330-011-2188-1
18. Cademartiri F, van der Lugt A, Luccichenti G, Pavone P, Krestin GP (2002) Parameters affecting bolus geometry in CTA: a review. J Comput Assist Tomogr 26(4):598–607, doi:00004728-200207000-00022 [pii]
19. de Monye C, de Weert TT, Zaalberg W, Cademartiri F, Siepman DA, Dippel DW, van der Lugt A (2006) Optimization of CT angiography of the carotid artery with a 16-MDCT scanner: craniocaudal scan direction reduces contrast material-related perivenous artifacts. AJR Am J Roentgenol 186(6):1737–1745. doi:10.2214/AJR.05.0143, 186/6/1737 [pii]
20. Liu Y, Hopper KD, Mauger DT, Addis KA (2000) CT angiographic measurement of the carotid artery: optimizing visualization by manipulating window and level settings and contrast material attenuation. Radiology 217(2):494–500
21. de Weert TT, Ouhlous M, Zondervan PE, Hendriks JM, Dippel DW, van Sambeek MR, van der Lugt A (2005) In vitro characterization of atherosclerotic carotid plaque with multidetector computed tomography and histopathological correlation. Eur Radiol 15(9):1906–1914. doi:10.1007/s00330-005-2712-2
22. van Straten M, Venema HW, Streekstra GJ, Majoie CB, den Heeten GJ, Grimbergen CA (2004) Removal of bone in CT angiography of the cervical arteries by piecewise matched mask bone elimination. Med Phys 31(10):2924–2933
23. Venema HW, Hulsmans FJ, den Heeten GJ (2001) CT angiography of the circle of Willis and intracranial internal carotid arteries: maximum intensity projection with matched mask bone elimination-feasibility study. Radiology 218(3):893–898
24. Uotani K, Watanabe Y, Higashi M, Nakazawa T, Kono AK, Hori Y, Fukuda T, Kanzaki S, Yamada N, Itoh T, Sugimura K, Naito H (2009) Dual-energy CT head bone and hard plaque removal for quantification of calcified carotid stenosis: utility and comparison with digital subtraction angiography. Eur Radiol 19(8):2060–2065. doi:10.1007/s00330-009-1358-x
25. Elgersma OE, Buijs PC, Wust AF, van der Graaf Y, Eikelboom BC, Mali WP (1999) Maximum internal carotid arterial stenosis: assessment with rotational angiography versus conventional intraarterial digital subtraction angiography. Radiology 213(3):777–783
26. Koelemay MJ, Nederkoorn PJ, Reitsma JB, Majoie CB (2004) Systematic review of computed tomographic angiography for assessment of carotid artery disease. Stroke 35(10):2306–2312. doi:10.1161/01.STR.0000141426.63959.cc, 01.STR.0000141426.63959.cc [pii]
27. Hollingworth W, Nathens AB, Kanne JP, Crandall ML, Crummy TA, Hallam DK, Wang MC, Jarvik JG (2003) The diagnostic accuracy of computed tomography angiography for traumatic or atherosclerotic lesions of the carotid and vertebral arteries: a systematic review. Eur J Radiol 48(1):88–102, doi:S0720048X03002006 [pii]
28. Bossuyt PM, Reitsma JB, Bruns DE, Gatsonis CA, Glasziou PP, Irwig LM, Lijmer JG, Moher D, Rennie D, de Vet HC, Standards for Reporting of Diagnostic Accuracy (2003) Towards complete and accurate reporting of studies of diagnostic accuracy: the STARD initiative. Clin Radiol 58(8):575–580, doi:S0009926003002587 [pii]
29. Wardlaw JM, Chappell FM, Best JJ, Wartolowska K, Berry E, NHS Research and Development Health Technology Assessment Carotid Stenosis Imaging Group (2006) Non-invasive imaging compared with intra-arterial angiography in the diagnosis of symptomatic carotid stenosis: a meta-analysis. Lancet 367(9521):1503–1512. doi:10.1016/S0140-6736(06)68650-9, S0140-6736(06)68650-9 [pii]
30. Chappell FM, Wardlaw JM, Young GR, Gillard JH, Roditi GH, Yip B, Pell JP, Rothwell PM, Brown MM, Gough MJ, Randall MS (2009) Carotid artery stenosis: accuracy of noninvasive tests – individual patient data meta-analysis. Radiology 251(2):493–502. doi:10.1148/radiol.2512080284, 2512080284 [pii]
31. Josephson SA, Bryant SO, Mak HK, Johnston SC, Dillon WP, Smith WS (2004) Evaluation of carotid stenosis using CT angiography in the initial evaluation of stroke and TIA. Neurology 63(3):457–460, doi:63/3/457 [pii]
32. Hacklander T, Wegner H, Hoppe S, Danckworth A, Kempkes U, Fischer M, Mertens H, Caldwell JH (2006) Agreement of multislice CT angiography and MR angiography in assessing the degree of carotid artery stenosis in consideration of different methods of postprocessing. J Comput Assist Tomogr 30(3):433–442, doi:00004728-200605000-00014 [pii]
33. Howard P, Bartlett ES, Symons SP, Fox AJ, Aviv RI (2010) Measurement of carotid stenosis on computed tomographic angiography: reliability depends on postprocessing technique. Can Assoc Radiol J 61(3):127–132. doi:10.1016/j.carj.2009.10.013, S0846-5371(09)00220-4 [pii]
34. Puchner S, Popovic M, Wolf F, Reiter M, Lammer J, Bucek RA (2009) Multidetector CTA in the quantification of internal carotid artery stenosis: value of different reformation techniques and axial source images compared with selective carotid arteriography. J Endovasc Ther 16(3):336–342. doi:10.1583/08-2636.1, 08-2636 [pii]
35. Kirbas C, Quek F (2004) A review of vessel extraction techniques and algorithms. ACM Comput Surv 36(2):81–121. doi:10.1145/1031120.1031121
36. Lesage D, Angelini ED, Bloch I, Funka-Lea G (2009) A review of 3D vessel lumen segmentation techniques: models, features and extraction schemes. Med Image Anal 13(6):819–845. doi:10.1016/j.media.2009.07.011, S1361-8415(09)00067-X [pii]
37. Manniesing R, Schaap M, Rozie S, Hameeteman R, Vukadinovic D, van der Lugt A, Niessen W (2010) Robust CTA lumen segmentation of the atherosclerotic carotid artery bifurcation in a large patient population. Med Image Anal 14(6):759–769. doi:10.1016/j.media.2010.05.001, S1361-8415(10)00046-0 [pii]
38. Manniesing R, Viergever MA, Niessen WJ (2007) Vessel axis tracking using topology constrained surface evolution. IEEE Trans Med Imaging 26(3):309–316. doi:10.1109/TMI.2006.891503
39. Milwer MB, Valencia LF, Hoyos MH, Magnin IE, Orkisz M (2007) Fast-marching contours for the segmentation of vessel lumen in CTA cross-sections. Conf Proc IEEE Eng Med Biol Soc 2007:791–794. doi:10.1109/IEMBS.2007.4352409
40. Cuisenaire O, Virmani S, Olszewski M, Ardon R (2008) Fully automated segmentation of carotid and vertebral arteries from contrast enhanced CTA. In: Reinhardt (ed) Med imaging 2008: image processing, SPIE. pp R–R-8. doi:10.1117/12.770481
41. Hameeteman K, Zuluaga MA, Freiman M, Joskowicz L, Cuisenaire O, Valencia LF, Gulsun MA, Krissian K, Mille J, Wong WC, Orkisz M, Tek H, Hoyos MH, Benmansour F, Chung AC, Rozie S, van Gils M, van den Borne L, Sosna J, Berman P, Cohen N, Douek PC, Sanchez I, Aissat M, Schaap M, Metz CT, Krestin GP, van der Lugt A, Niessen WJ, van Walsum T (2011) Evaluation framework for carotid bifurcation lumen segmentation and stenosis grading. Med Image Anal 15(4):477–488. doi:10.1016/j.media.2011.02.004, S1361-8415(11)00026-0 [pii]
42. Scherl H, Hornegger J, Prummer M, Lell M (2007) Semi-automatic level-set based segmentation and stenosis quantification

of the internal carotid artery in 3D CTA data sets. Med Image Anal 11(1):21–34. doi:10.1016/j.media.2006.09.004, S1361-8415(06)00076-4 [pii]
43. Wintermark M, Glastonbury C, Tong E, Lau BC, Schaeffer S, Chien JD, Haar PJ, Saloner D (2008) Semi-automated computer assessment of the degree of carotid artery stenosis compares favorably to visual evaluation. J Neurol Sci 269(1–2):74–79. doi:10.1016/j.jns.2007.12.023, S0022-510X(07)00816-7 [pii]
44. Berg M, Zhang Z, Ikonen A, Manninen H, Vanninen R (2005) Carotid stenosis assessment with CT angiography using advanced vessel analysis software. Int Congr Ser 1281:322–327
45. Zhang Z, Berg M, Ikonen A, Kononen M, Kalviainen R, Manninen H, Vanninen R (2005) Carotid stenosis degree in CT angiography: assessment based on luminal area versus luminal diameter measurements. Eur Radiol 15(11):2359–2365. doi:10.1007/s00330-005-2801-2
46. Groen HC, Gijsen FJ, van der Lugt A, Ferguson MS, Hatsukami TS, van der Steen AF, Yuan C, Wentzel JJ (2007) Plaque rupture in the carotid artery is localized at the high shear stress region: a case report. Stroke 38(8):2379–2381. doi:10.1161/STROKEAHA.107.484766, STROKEAHA.107.484766 [pii]
47. Lee SW, Antiga L, Spence JD, Steinman DA (2008) Geometry of the carotid bifurcation predicts its exposure to disturbed flow. Stroke 39(8):2341–2347. doi:10.1161/STROKEAHA.107.510644, STROKEAHA.107.510644 [pii]
48. Cademartiri F, Mollet NR, Runza G, Bruining N, Hamers R, Somers P, Knaapen M, Verheye S, Midiri M, Krestin GP, de Feyter PJ (2005) Influence of intracoronary attenuation on coronary plaque measurements using multislice computed tomography: observations in an ex vivo model of coronary computed tomography angiography. Eur Radiol 15(7):1426–1431. doi:10.1007/s00330-005-2697-x
49. Romero JM, Babiarz LS, Forero NP, Murphy EK, Schaefer PW, Gonzalez RG, Lev MH (2009) Arterial wall enhancement overlying carotid plaque on CT angiography correlates with symptoms in patients with high grade stenosis. Stroke 40(5):1894–1896. doi:10.1161/STROKEAHA.108.529008, STROKEAHA.108.529008 [pii]
50. Saba L, Mallarini G (2011) Carotid plaque enhancement and symptom correlations: an evaluation by using multidetector row CT angiography. AJNR Am J Neuroradiol 32(10):1919–1925. doi:10.3174/ajnr.A2605, ajnr.A2605 [pii]
51. Streifler JY, Eliasziw M, Fox AJ, Benavente OR, Hachinski VC, Ferguson GG, Barnett HJ (1994) Angiographic detection of carotid plaque ulceration. Comparison with surgical observations in a multicenter study. North American Symptomatic Carotid Endarterectomy Trial. Stroke 25(6):1130–1132
52. Randoux B, Marro B, Koskas F, Duyme M, Sahel M, Zouaoui A, Marsault C (2001) Carotid artery stenosis: prospective comparison of CT, three-dimensional gadolinium-enhanced MR, and conventional angiography. Radiology 220(1):179–185
53. Walker LJ, Ismail A, McMeekin W, Lambert D, Mendelow AD, Birchall D (2002) Computed tomography angiography for the evaluation of carotid atherosclerotic plaque: correlation with histopathology of endarterectomy specimens. Stroke 33(4):977–981
54. Saba L, Caddeo G, Sanfilippo R, Montisci R, Mallarini G (2007) Efficacy and sensitivity of axial scans and different reconstruction methods in the study of the ulcerated carotid plaque using multidetector-row CT angiography: comparison with surgical results. AJNR Am J Neuroradiol 28(4):716–723, doi:28/4/716 [pii]
55. de Weert TT, Cretier S, Groen HC, Homburg P, Cakir H, Wentzel JJ, Dippel DW, van der Lugt A (2009) Atherosclerotic plaque surface morphology in the carotid bifurcation assessed with multidetector computed tomography angiography. Stroke 40(4):1334–1340. doi:10.1161/STROKEAHA.108.538439, STROKEAHA.108.538439 [pii]
56. Wintermark M, Jawadi SS, Rapp JH, Tihan T, Tong E, Glidden DV, Abedin S, Schaeffer S, Acevedo-Bolton G, Boudignon B, Orwoll B, Pan X, Saloner D (2008) High-resolution CT imaging of carotid artery atherosclerotic plaques. AJNR Am J Neuroradiol 29(5):875–882. doi:10.3174/ajnr.A0950, ajnr.A0950 [pii]
57. Estes JM, Quist WC, Lo Gerfo FW, Costello P (1998) Noninvasive characterization of plaque morphology using helical computed tomography. J Cardiovasc Surg (Torino) 39(5):527–534
58. Oliver TB, Lammie GA, Wright AR, Wardlaw J, Patel SG, Peek R, Ruckley CV, Collie DA (1999) Atherosclerotic plaque at the carotid bifurcation: CT angiographic appearance with histopathologic correlation. AJNR Am J Neuroradiol 20(5):897–901
59. de Weert TT, Ouhlous M, Meijering E, Zondervan PE, Hendriks JM, van Sambeek MR, Dippel DW, van der Lugt A (2006) In vivo characterization and quantification of atherosclerotic carotid plaque components with multidetector computed tomography and histopathological correlation. Arterioscler Thromb Vasc Biol 26(10):2366–2372. doi:10.1161/01.ATV.0000240518.90124.57, 01.ATV.0000240518.90124.57 [pii]
60. Agatston AS, Janowitz WR, Hildner FJ, Zusmer NR, Viamonte M Jr, Detrano R (1990) Quantification of coronary artery calcium using ultrafast computed tomography. J Am Coll Cardiol 15(4):827–832, doi:0735-1097(90)90282-T [pii]
61. Kwee RM (2010) Systematic review on the association between calcification in carotid plaques and clinical ischemic symptoms. J Vasc Surg 51(4):1015–1025. doi:10.1016/j.jvs.2009.08.072, S0741-5214(09)01788-1 [pii]
62. de Weert TT, de Monye C, Meijering E, Booij R, Niessen WJ, Dippel DW, van der Lugt A (2008) Assessment of atherosclerotic carotid plaque volume with multidetector computed tomography angiography. Int J Cardiovasc Imaging 24(7):751–759. doi:10.1007/s10554-008-9309-1
63. Vukadinovic D, van Walsum T, Manniesing R, Rozie S, Hameeteman R, de Weert TT, van der Lugt A, Niessen WJ (2010) Segmentation of the outer vessel wall of the common carotid artery in CTA. IEEE Trans Med Imaging 29(1):65–76. doi:10.1109/TMI.2009.2025702
64. Vukadinovic D, Rozie S, van Gils M, van Walsum T, Manniesing R, van der Lugt A, Niessen WJ (2011) Automated versus manual segmentation of atherosclerotic carotid plaque volume and components in CTA: associations with cardiovascular risk factors. Int J Cardiovasc Imaging 28(4):877–887. doi:10.1007/s10554-011-9890-6
65. Rozie S, de Weert TT, de Monye C, Homburg PJ, Tanghe HL, Dippel DW, van der Lugt A (2009) Atherosclerotic plaque volume and composition in symptomatic carotid arteries assessed with multidetector CT angiography; relationship with severity of stenosis and cardiovascular risk factors. Eur Radiol 19(9):2294–2301. doi:10.1007/s00330-009-1394-6
66. Homburg PJ, Rozie S, van Gils MJ, van den Bouwhuijsen QJ, Niessen WJ, Dippel DW, van der Lugt A (2011) Association between carotid artery plaque ulceration and plaque composition evaluated with multidetector CT angiography. Stroke 42(2):367–372. doi:10.1161/STROKEAHA.110.597369, STROKEAHA.110.597369 [pii]
67. Wintermark M, Arora S, Tong E, Vittinghoff E, Lau BC, Chien JD, Dillon WP, Saloner D (2008) Carotid plaque computed tomography imaging in stroke and nonstroke patients. Ann Neurol 64(2):149–157. doi:10.1002/ana.21424
68. Nandalur KR, Hardie AD, Raghavan P, Schipper MJ, Baskurt E, Kramer CM (2007) Composition of the stable carotid plaque: insights from a multidetector computed tomography study of plaque volume. Stroke 38(3):935–940. doi:10.1161/01.STR.0000257995.74834.92, 01.STR.0000257995.74834.92 [pii]